Resolving a Guanine-Quadruplex Structure in the SARS-CoV-2 Genome through Circular Dichroism and Multiscale Molecular Modeling.

Luisa D'Anna,[a] Tom Miclot,[a,b] Emmanuelle Bignon,[b] Ugo Perricone,[c] Giampaolo Barone,[a,*] Antonio Monari,[d,*] Alessio Terenzi[a,*]

a) Department of Biological, Chemical and Pharmaceutical Sciences, University of Palermo, 90126 Palermo, Italy; b) Université de Lorraine and CNRS, UMR 7019 LPCT, F-54000 Nancy, France; c) Fondazione Ri.MED, Via Filippo Marini 14, 90128, Palermo, Italy d) Université Paris Cité and CNRS, ITODYS F-75006 Paris, France

SARS-CoV-2, RNA viruses, genome organization, Guanine quadruplexes, electronic circular dichroism, molecular modeling and simulation.

ABSTRACT: The genome of SARS-CoV-2 coronavirus is made up of a single-stranded RNA fragment that can assume a specific secondary structure, whose stability can influence the virus ability to reproduce. Recent studies have identified putative guanine quadruplex sequences in SARS-CoV-2 genome fragments that are involved in coding for both structural and non-structural proteins. In this contribution, we focus on a specific G-rich sequence referred as RG-2, which codes for the non-structural protein 10 (Nsp10) and assumes a parallel guanine-quadruplex (G4) arrangement. We provide the secondary structure of the RG-2 G4 at atomistic resolution by molecular modeling and simulation, validated by the superposition of experimental and calculated electronic circular dichroism spectrum. Through both experimental and simulation approaches, we have demonstrated that pyridostatin (PDS), a widely recognized G4 binder, can bind to and stabilize RG-2 G4 more strongly than RG-1, another G4 forming sequence that was previously proposed as a potential target for antiviral drug candidates. Overall, this study highlights RG-2 as a valuable target to inhibit the translation and replication of SARS-CoV-2 paving the way towards original therapeutic approaches against emerging RNA viruses.

The outbreak and evolution of the COVID-19 pandemics,[1–4] caused by SARS-CoV-2 virus, has dramatically evidenced the risks related to emerging infectious diseases and the necessity to understand, at a molecular level, the complex mechanisms behind viral replication and reproduction. RNA viruses, including coronaviruses, can be counted among the most problematic emerging infectious diseases, due to their adaptability, high mutation rate, and transmissibility. A deep understanding of RNA viruses functioning, which in turn allows the rapid deployment of pharmaceuticals or vaccinal measures in case of an epidemic or pandemic event, is therefore highly needed.

SARS-CoV-2 viral genome is composed of a relatively large positive-sensed RNA strand of about 300k nucleobases. Upon cellular infection, and the entry into the host compartments, the genome is directly translated by cellular ribosome to produce the viral proteins which will further allow the reproduction of the virus and the diffusion of the infection. The sequencing and characterization of SARS-CoV-2 genome revealed that it codes for both structural proteins, including the well-known Spike (S),[5,6] and non-structural proteins (Nsp) exerting enzymatic activity and favoring the viral maturation or its protection via the evasion of the host immune system.[7–10] Among the non-structural proteins there are the viral proteases,[11,12] which participate into the maturation of the originally produced large polyprotein, and the RNA-dependent RNA polymerase which, duplicating the viral RNA, allows its replication.[9,13,14] Both proteins represent a key target for antiviral agents and have been largely studied by molecular and structural biology as well as simulation approaches.[13–15]

Despite its apparent simplicity, the genomic organization of RNA viruses hinders some level of complexity, often correlated with the virus reproductive capacity and infectivity.[16–19] RNA and DNA viruses, including flaviviruses,[20] Zika,[21] Dengue,[22] and human immunodeficiency viruses (HIV),[23] possess putative guanine quadruplex sequences (PQS).[24,25] These G-rich sequences are associated to crucial regulatory roles, especially in the framework of gene expression. Furthermore, the interplay between guanine quadruplexes of the host cells and the viral protein machinery has important consequences on the virus lifecycle. For instance, specific viral Nsp are activated by the interaction with guanine quadruplexes.[26,27] The stabilization of such motifs with specific ligands hampers the replication or translation of the viral genome, blocking or slowing the viral infection.[28,29] Thus, this approach represents an interesting and alternative therapeutic strategy to counteract emerging infectious diseases.[20,30]

Guanine quadruplexes (G4s) are arrangements forming in guanine-rich regions of RNA and DNA.[24,31] They consist of π-stacked tetrads of four guanine locked by Hoogsteen-type hydrogen bonds.[32] The guanines composing the tetrad do not need to be contiguous in the sequence and may be bridged by rather large and flexible loops. G4s are further stabilized by monovalent cations, usually Na^+ or K^+, which occupy the central

channel generated by the stacked tetrads.[33,34] In addition, G4s exist under different topologies, parallel, hybrid and antiparallel, depending on the relative orientation of the connecting strands and of the glycosidic bonds. While these three topologies have been all observed in DNA G4s, RNA G4s have a marked preference for the parallel arrangement.[31,35] Parallel, antiparallel and hybrid G4 topologies are characterized by specific signatures in their electronic circular dichroism (ECD) spectra, thus allowing their recognition and characterization.[36–39]

Some PQS sequences have been recently spotlighted in SARS-CoV-2 genome.[29,40–42] Qu et al.,[29] focused their studies on one particular sequence, named RG-1, which codes for the nucleocapsid (N) protein, and is located in the region 28,903-28,917 of the viral genome. The stable G4 arrangement of RG-1 has been confirmed by ECD measurements[29,40] and its precise atomic-scale structure has been predicted by our group using a multiscale simulation approach combining classical molecular dynamics (MD) simulations and hybrid quantum mechanics/molecular mechanics (QM/MM) techniques.[43] Very recently, Qu et al. published a study on another PQS located in the region 3,467-3,483, forming a G4 which is more stable than RG-1 and suggested that this could be the target of a known G4 binder (TMPyP4) able to suppresses SARS-CoV-2 infection in an infected animal model.[29]

A further PQS, labelled as RG-2, was identified in the region 13,385-13,404 and it codes for the Nsp10 of SARS-CoV-2.[29,40–42] However, Qu et al,[29] reasoning that RG-2 quadruplex is less stable than RG-1 and other G4s of the SARS-CoV-2 genome, do not consider it as valuable target for antiviral agents and they set it aside. On the contrary, we strongly believe that RG-2 could represent a more valuable target for G4-aimed drugs since it is more prone to stabilization. Furthermore, Nsp10 has a crucial role in assuring the viral maturation and represents a fundamental cofactor in the activation of multiple replicative enzymes.[44] Indeed, the formation of a complex with Nsp10 is necessary to assure the exoribonuclease activity of Nsp14, which constitutes a proof-reading step avoiding RNA replication errors.[45] Nsp10 is also necessary to assure the methyltransferase capacity of Nsp16, which increases the RNA stability by its capping with a methyl group.[46] The indirect inhibition of the replication and repair-capacity of Nsp14 by targeting the RG-2 G4 may also increase the efficiency of nucleoside-analogous antiviral agents.

Globally, the possibility to develop G4-targeted antiviral agents against emerging infectious diseases, and RNA viruses in particular, is highly appealing.[40] However, to assure a rational design of the potential therapeutic agents, hence to maximize their efficiency and selectivity, it is necessary to obtain a proper atomistic-resolved structure of the involved targets. In this respect, the determination of RNA secondary structures may be challenging also due to the inherent instability of RNA oligomers. In a previous contribution[43] we have reported a multiscale approach which has confirmed the G4 arrangement of the SARS-CoV-2 RG-1 sequence, providing its full-atom structure. This was achieved by long-range MD simulations on a starting guess arrangement obtained by sequence alignment between RG-1 and other G4 sequences. The simulation of the ECD spectrum on top of snapshots issued by the MD simulation has provided a one-to-one mapping with the experimental results, confirming the soundness of the proposed model-structure.[43]

In the present contribution we provide the first structural resolution prediction of the RG-2 G4 in SARS-CoV-2, relying on ECD spectroscopy and exploiting a similar computational protocol to describe its arrangement at the atomic-level. The simulated ECD spectra, obtained at hybrid quantum mechanics/ molecular mechanics (QM/MM) level is also used to support the soundness and robustness of the computational model. In addition, the stabilization of the G4 arrangement of RG-2 also in comparison with RG-1, by pyridostatin (PDS), a well-known G4-ligand,[47] is assessed by FRET melting analysis and ECD. The full experimental and computational protocols are reported and discussed in the Electronic Supplementary Information (ESI).

The RG-2 segment of the SARS-CoV-2 genome is a guanine rich area in the Nsp10 coding-region and is characterized by the 3'-GGUAUGUGGAAAGGUUAUGG-5' primary sequence.[29,40–42] The alignment between RG-2 and different G4-forming sequences has been performed and the maximum similarity has been obtained with the telomeric DNA sequence (PDB code 3DCM).[48] Therefore, the former has been chosen as a starting template, after converting DNA to RNA. Subsequently, two independent MD replicas, each exceeding the μs-time scale, have been performed, using the NAMD code.[49,50]

After a slight structural reorganization observed in the very first steps of the simulation, RG-2 evolves towards a stable parallel G4 arrangements composed of two stacked tetrads and stabilized by a central K^+ ion (Figure 1).

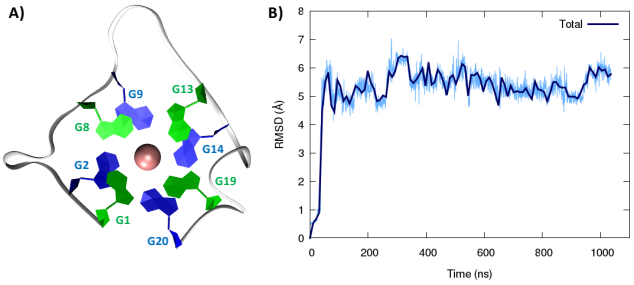

Figure 1. A Representative snapshot of the parallel G4 formed by the RG-2 sequence as obtained by MD simulations. Guanine residues composing the two superposing tetrads are evidenced by different colors (A). The corresponding time series of the RMSD for the RNA strand (B). Analogous results obtained for the second replica are reported in ESI.

As seen in Figure 1A, the first tetrad is composed by G1, G8, G13, and G19. The residues G2, G9, G14, and G20 constitute the second tetrad. The stability and the rigidity of the structure can be also appreciated by the time evolution of the Root Mean Square Deviation (RMSD), which is reported in Figure 1B, and which after the initial increase remains stable throughout the whole simulation. The two tetrads are bridged by rather short, yet still flexible unstructured loop. Interestingly, this aspect constitutes a significant difference with the RG-1 sequence, which instead presents a long and extremely flexible loop responsible for the global G4 conformational flexibility.[43]

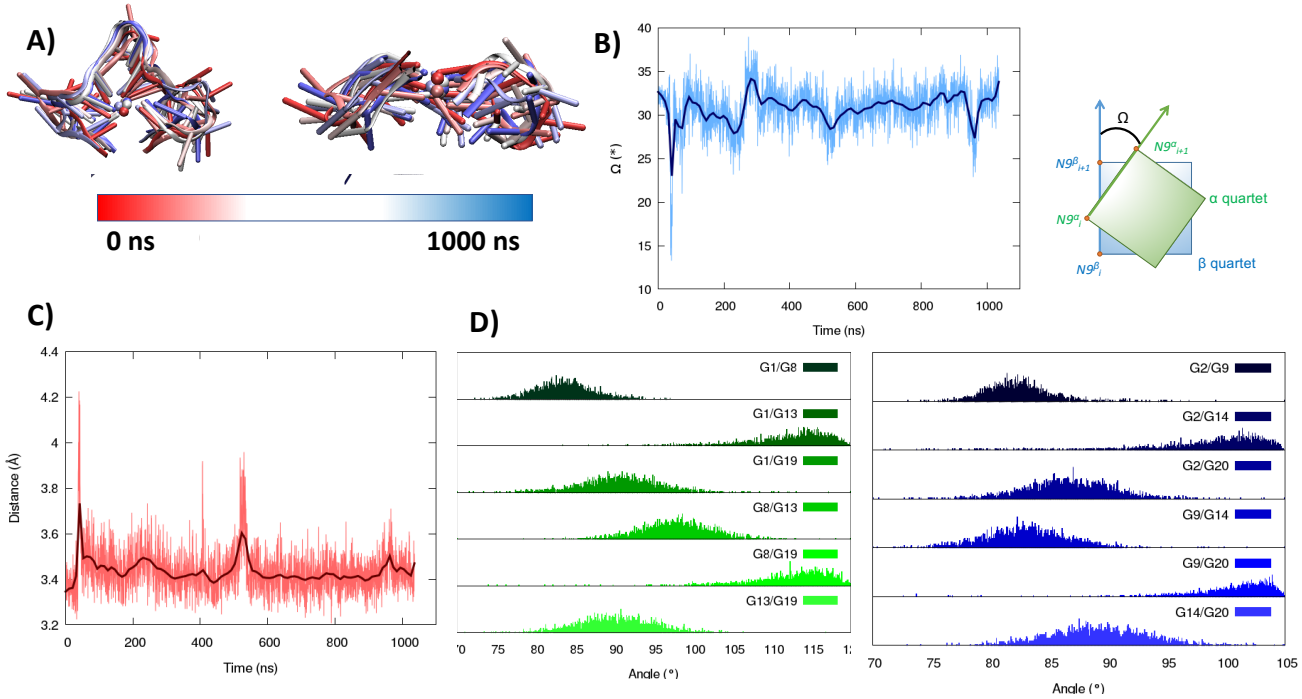

Figure 2. Evolution of the structure of RG-2 along the MD simulation in top and front view (A). Time series of the twist angle W between the tetrad and its geometrical definition (B). Time series of the distance between the tetrads (C). Distribution of the angles between the axis of the guanines composing the first, green, and the second, blue, tetrad (D). Analogous results obtained for the second replica are reported in ESI.

The absence of long peripheral loops is enhancing the rigidity of the RG-2 arrangement, while providing a globally more compact structure as can be seen in the superposition of the snapshots extracted from the MD trajectory shown in Figure 2A. Unsurprisingly, the G4 arrangement also leads to a rather rigid core, whose structural parameters are close to the ideal geometry. The two G4 tetrads experience a twist angle between their axis close to ideality averaging at 30.8±2° for the first replica (Figure 2B) and at 29.0±2° for the second one. The same rigidity can also be appreciated by the distance between the center of mass of the two tetrads, which also shows a very limited evolution and oscillation all along the simulation comprised between 3.43±0.09 and 3.45±0.08 Å, for the first and the second replica, respectively (Figure 2C). These values are also coherent with near ideal π-stacking between the tetrads, globally confirming the overall stability of the aggregate. Finally, as can be appreciated in Figure 2D, the twist angle between the main axis of the tetrad-forming guanine residues is also rather rigid, as exemplified by the limited spread of the distribution.

To confirm the G4-arrangement of RG-2 we recorded the ECD spectrum of the corresponding G-rich sequence folded in K^+ containing solution and compared to the simulated one (Figure 3). The experimental spectrum exhibits a weak negative band at 240 nm, a strong positive ellipticity at 260 nm followed by a positive shoulder at 290 nm. Our result is more in line with the one published by Zhang et al.,[42] while Qu and collaborators, in both of their papers,[29,40] do not report about the presence of the shoulder at around 290 nm. The band at 260 nm is consistent with anti–anti guanine base steps typical of parallel quadruplexes while the shoulder at 290 nm reveals an antiparallel character,[51] which is quite uncommon for RNA quadruplex with an exception represented by the artificial RNA aptamer *Spinach*.[52]

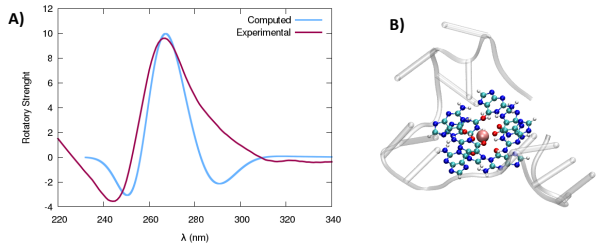

Figure 3. Comparison between the experimental and simulated QM/MM ECD spectrum of RG-2 in water solution (A). The computed spectrum is simulated by QM/MM calculations, using the M06-2X functional, similar results are obtained using the ωB97XD, see ESI. To reproduce the experimental signal a broadening factor of 0.15 eV has been applied to each vertical transition. The QM partition is illustrated in panel B in ball and stick representations and comprises all the nucleobases forming the tetrads and the central K^+ ion.

Notwithstanding the equilibrium, the predominant topology in K^+ buffer is clearly the parallel one. The simulated spectrum, which is obtained considering the evolution of the sequence geometry along the MD simulation for the parallel arrangement, matches satisfactorily with the shape of the experimental ECD, thus confirming the soundness of our atomistic model. However, the shoulder appearing at around 290 nm is missing, coherently with the fact that our model only involves a parallel arrangement, while the ensuing negative signal at around 240 nm is slightly underestimated in our simulation.

Globally, our results confirm the predominance of the parallel arrangement and the possible presence of a minoritarian anti-parallel folding. We note that a shift of the absorption wavelengths has been applied to the calculated spectrum. As already discussed in our previous contribution,[43] the blue-shifted computed ECD signal is mainly due to incomplete basis set but does not prevent comparing the shape of the main transition to validate the structure topology assignation.

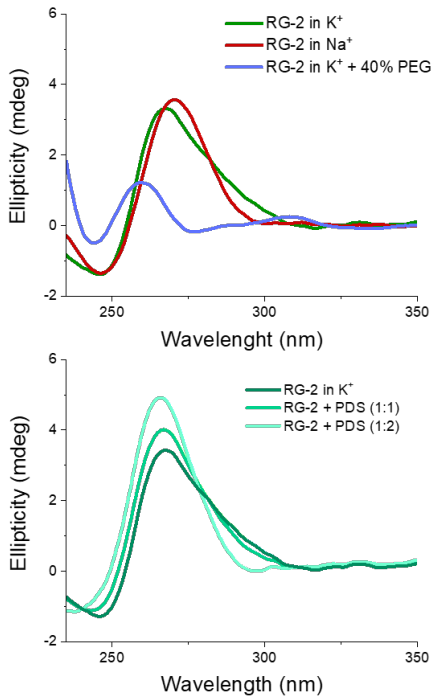

Figure 4. Upper panel: experimental ECD spectra of RG-2 in K^+ or Na^+ containing buffers and in the presence of PEG-200 as crowding agent. Lower panel: experimental ECD spectrum of RG-2 in K^+ in the presence of increasing concentration of PDS.

We also recorded the ECD spectrum of RG-2 sequence in Na^+ containing buffer and in the presence of PEG-200 as crowding agent. While the main signature of a parallel G4 is maintained in Na^+ ions as confirmed by the presence of the strong positive band at 260 nm, (Figure 4), the shoulder at 290 nm is no longer observed, indicating that the equilibrium between the parallel/antiparallel topology is totally shifted toward the first occurrence. Interestingly, the ECD recorded in K^+ buffer with 40% PEG-200 shows a noticeable shift for the positive band at 258 nm and the presence of a weaker band at around 300 nm. These features are typical of an antiparallel topology of group III, according to the classification proposed by Webba da Silva and collaborators.[51]

We also recorded the spectra of RG-2 in the different buffers in the presence of the known G4 binder PDS to observe possible conformational changes. Two different [RNA]:[PDS] ratios were used (1:1 and 1:2, respectively). As reported in Figure 4 (lower panel), when PDS is added to RG-2 in K^+ buffer the intensity of the ECD band increases according to the concentration of the ligand followed by the disappearance of the shoulder at 290 nm. This result indicates the stabilization of RG-2 in its parallel topology. In Na^+ buffer, the increasing concentration of PDS does not produce any conformational change of the G4 which remains in its parallel arrangement. In the presence of the crowding agent, PDS increases the intensity of the ECD bands, which is associated with a slight shift to higher wavelengths, possibly indicating the beginning of a switch toward the parallel arrangement of the G4. The formation of a stable aggregate between RG-2 and PDS has also been confirmed by MD simulations as shown in Figure 5. Indeed, after equilibration, PDS is rapidly attracted toward the G4 and forms a highly stable complex via π-stacking with the exposed tetrads. Interestingly, the time evolution of the distance between the center of mass of PDS and of the tetrad-forming guanines remains remarkably stable for a time-laps exceeding the μs scale. The structural parameters of the G4-folded RG2 are only slightly perturbed by the presence of PDS (see ESI), justifying the experimentally observed similarity between the ECD spectra.

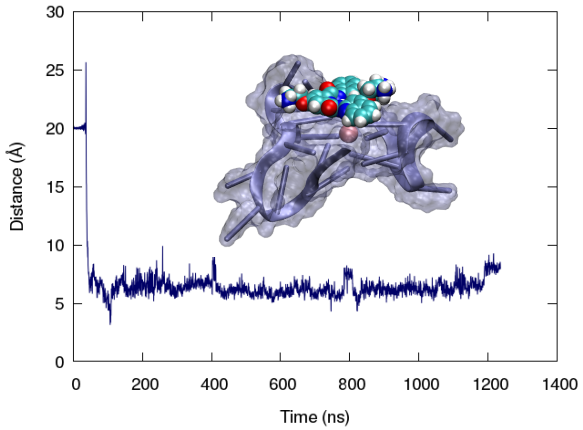

Figure 5. Time evolution of the distance between the centers of mass of PDS and the guanine-forming tetrads of the RG-2 sequence along equilibrium MD simulation. A representative snapshot is also provided in the inlay, the G4 is represented in cartoon and transparent surface representation while PDS is displayed in van der Waals style.

As mentioned before, Qu et al.,[40] comparing RG-2 and RG-1 G4 melting temperatures measured by ECD, concluded that RG-2 is less stable under physiological conditions showing a T_m around 45 °C. For this reason, the authors focused their studies on RG-1 only, deeming this G4 a better target for antiviral drug candidates. We performed Forster Resonance Energy Transfer (FRET) melting assay using RG-1 and RG-2 oligonucleotides, modified with a fluorophore (FAM) and a quencher (TAMRA) at the 5' and 3' ends, respectively, alone or in presence of increasing concentration of PDS. Contrary to what reported by Qu et al.,[29] in our experiment RG-1 and RG-2 have almost the same melting temperature (51.8 and 50.6 °C, respectively), which is thus compatible with G4 folding in physiological conditions. The difference with data from Qu et al.[29] can be attributed to the slightly different experimental conditions (type of buffer, K^+ concentration and presence of fluorophores). However, and interestingly, the RG-2 quadruplex is stabilized more efficiently by PDS when compared to RG-1 both at 1:5 and 1:10 [RNA]:[PDS] ratios (Figure S6 and Figure 6, respectively). Therefore, its targeting for antiviral purposes appears highly suitable.

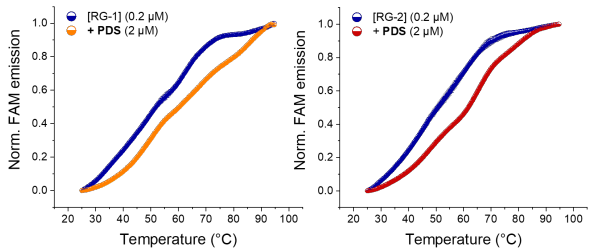

Figure 6. FRET melting curves of RG-1 and RG-2 (potassium cacodylate buffer, pH = 7.4) in the presence of PDS.

In this contribution we present the first structural prediction of a SARS-CoV-2 genome sequence involved in coding the Nsp10 protein, which is essential for viral replication. In particular, we have shown that RG-2 assumes a parallel G4 arrangement, composed of two rigid tetrads, almost ideally π-stacked, bridged by short, yet flexible loops. The simulation of the ECD spectrum and its comparisons with the experimental data validates our structural model at an atomistic level. Interestingly, the experimental ECD spectra points to the presence, in K^+ buffer, of a minoritarian antiparallel folding. This result is quite surprising yielding one of the very few RNA G4 able to experience polymorphism and assume topologies different from the parallel folding. Remarkably, PDS switches the equilibrium completely toward the parallel arrangement.

We confirm that our protocol, based on the combination of multiscale modeling, including sequence homology, MD simulations, and in silico spectroscopy, combined with experimental ECD spectroscopy represents a very suitable solution for the proposition of secondary structures in the genome of emerging viruses. Thus, it will offer a robust strategy for the rational development of antivirals targeting emerging infectious diseases.

We have also shown by ECD and FRET that the well-known G4-binder PDS stabilizes the RG-2 secondary structure more efficiently than RG-1, offering a valuable antiviral strategy against emerging RNA viruses. Indeed, the stabilization of RG-2 G4 would result in the inhibition of the RNA translation and replication, and hence will hamper the viral diffusion. This is particularly true since Nsp10, which RG-2 participates to encode, is involved in critical processes assuring SARS-CoV-2 fitness, and is related to the proof-reading of the RNA synthesized by the RNA-dependent-RNA-polymerase, and to the increase of its stability by methyl capping. In perspective, we aim at evaluating how Nsp10 expression changes in SARS-CoV-2 infected host cells to further validate RG-2 as a suitable target for COVID-19 treatment. Considering that G4 forming sequences, including RG-2, are highly conserved among coronaviruses,[42] our definitively paves the way for possible efficient treatment in the fight against new emerging viruses of this family.

ASSOCIATED CONTENT

Supporting Information

The Supporting Information is available free of charge on the ACS Publications website.

Extended experimental and computational methodology, RMSD and structural parameters for the second MD replica and the system containing PDS. FRET melting profiles of RG-1 and RG-2, and ECD spectra of RG-2 in presence of PDS (file type PDF) Pdb file extracted from the MD simulation showing the most populated clusters of RG-2 folded in parallel arrangement (file type PDB)

AUTHOR INFORMATION

Corresponding Author

* G.B. Giampaolo.barone@unipa.it, A. M. antonio.monari@u-paris.fr, A.T. Alessio.terenzi@unipa.it

Author Contributions

The manuscript was written through contributions of all authors. / All authors have given approval to the final version of the manuscript.

ACKNOWLEDGMENT

All the simulations have been performed on the LPCT, Explor, and GENCI computing resources which are gratefully acknowledge. Financial support from the French Ministry for Higher Education and Research (MESR) and CNRS is also acknowledged. A.M. thanks ANR and CGI for their financial support of this work through Labex SEAM ANR 11 LABX 086, ANR 11 IDEX 05 02. The support of the IdEx "Université Paris 2019" ANR-18-IDEX-0001.

REFERENCES

(1) Hu, B.; Guo, H.; Zhou, P.; Shi, Z. L. Characteristics of SARS-CoV-2 and COVID-19. *Nat. Rev. Microbiol.* **2021**, *19* (3), 141–154. https://doi.org/10.1038/s41579-020-00459-7.

(2) Dömling, A.; Gao, L. Chemistry and Biology of SARS-CoV-2. *Chem* **2020**, *6* (6), 1283–1295. https://doi.org/10.1016/j.chempr.2020.04.023.

(3) Liu, Y. C.; Kuo, R. L.; Shih, S. R. COVID-19: The First Documented Coronavirus Pandemic in History. *Biomed. J.* **2020**, *43* (4), 328–333. https://doi.org/10.1016/j.bj.2020.04.007.

(4) Harapan, H.; Itoh, N.; Yufika, A.; Winardi, W.; Keam, S.; Te, H.; Megawati, D.; Hayati, Z.; Wagner, A. L.; Mudatsir, M. Coronavirus Disease 2019 (COVID-19): A Literature Review. *J. Infect. Public Health* **2020**, *13* (5), 667–673. https://doi.org/10.1016/j.jiph.2020.03.019.

(5) Wrapp, D.; Wang, N.; Corbett, K. S.; Goldsmith, J. A.; Hsieh, C.-L. L.; Abiona, O.; Graham, B. S.; McLellan, J. S. Cryo-EM Structure of the 2019-NCoV Spike in the Prefusion Conformation. *Science (80-.).* **2020**, *367* (6483), 1260–1263. https://doi.org/10.1126/science.abb2507.

(6) Shang, J.; Ye, G.; Shi, K.; Wan, Y.; Luo, C.; Aihara, H.; Geng, Q.; Auerbach, A.; Li, F. Structural Basis of Receptor Recognition by SARS-CoV-2. *Nature* **2020**, *581* (7807), 221–224. https://doi.org/10.1038/s41586-020-2179-y.

(7) Cottam, E. M.; Whelband, M. C.; Wileman, T. Coronavirus NSP6 Restricts Autophagosome Expansion. *Autophagy* **2014**, *10* (8), 1426–1441. https://doi.org/10.4161/auto.29309.

(8) Kern, D. M.; Sorum, B.; Mali, S. S.; Hoel, C. M.; Sridharan, S.; Remis, J. P.; Toso, D. B.; Kotecha, A.; Bautista, D. M.; Brohawn, S. G. Cryo-EM Structure of SARS-CoV-2 ORF3a in Lipid Nanodiscs. *Nat. Struct. Mol. Biol.* **2021**, *28* (7), 573–582. https://doi.org/10.1038/s41594-021-00619-0.

(9) Hillen, H. S.; Kokic, G.; Farnung, L.; Dienemann, C.; Tegunov, D.; Cramer, P. Structure of Replicating SARS-CoV-2 Polymerase. *Nature* **2020**, *584* (7819), 154–156. https://doi.org/10.1038/s41586-020-2368-8.

(10) Chen, X.; Zhou, Z.; Huang, C.; Zhou, Z.; Kang, S.; Huang, Z.; Jiang, G.; Hong, Z.; Chen, Q.; Yang, M.; He, S.; Liu, S.; Chen, J.; Li, K.; Li, X.; Liao, J.; Chen, J.; Chen, S. Crystal Structures of Bat and Human Coronavirus ORF8 Protein Ig-Like Domain Provide Insights Into the Diversity of Immune Responses. *Front. Immunol.* **2021**, *12*. https://doi.org/10.3389/fimmu.2021.807134.

(11) Shin, D.; Mukherjee, R.; Grewe, D.; Bojkova, D.; Baek, K.; Bhattacharya, A.; Schulz, L.; Widera, M.; Mehdipour, A. R.; Tascher, G.; Geurink, P. P.; Wilhelm, A.; van der Heden van Noort, G. J.; Ovaa, H.; Müller, S.; Knobeloch, K.-P.; Rajalingam, K.; Schulman, B. A.; Cinatl, J.; Hummer, G.; Ciesek, S.; Dikic, I. Papain-like Protease Regulates SARS-CoV-2 Viral Spread and Innate Immunity. *Nature* **2020**, doi: 10.21203/rs.3.rs-27134/v1. https://doi.org/10.1038/s41586-020-2601-5.

(12) Muramatsu, T.; Takemoto, C.; Kim, Y. T.; Wang, H.; Nishii, W.; Terada, T.; Shirouzu, M.; Yokoyama, S. SARS-CoV 3CL Protease Cleaves Its C-Terminal Autoprocessing Site by Novel Subsite Cooperativity. *Proc. Natl. Acad. Sci. U. S. A.* **2016**. https://doi.org/10.1073/pnas.1601327113.

(13) Aranda, J.; Wieczór, M.; Terrazas, M.; Brun-Heath, I.; Orozco, M. Mechanism of Reaction of RNA-Dependent RNA Polymerase from SARS-CoV-2. *Chem Catal.* **2022**, *2* (5), 1084–1099. https://doi.org/10.1016/j.checat.2022.03.019.

(14) Bignon, E.; Monari, A. Modeling the Enzymatic Mechanism of the SARS-CoV-2 RNA-Dependent RNA Polymerase by DFT/MM-MD: An Unusual Active Site Leading to High Replication Rates. *J. Chem. Inf. Model.* **2022**, *62* (17), 4261–4269. https://doi.org/10.1021/acs.jcim.2c00802.

(15) Ramos-Guzmán, C. A.; Ruiz-Pernía, J. J.; Tuñón, I. Unraveling the SARS-CoV-2 Main Protease Mechanism Using Multiscale Methods. *ACS Catal.* **2020**, *10* (21), 12544–12554. https://doi.org/10.1021/acscatal.0c03420.

(16) Kadam, S. B.; Sukhramani, G. S.; Bishnoi, P.; Pable, A. A.; Barvkar, V. T. SARS-CoV-2, the Pandemic Coronavirus: Molecular and Structural Insights. *J. Basic Microbiol.* **2021**, *61* (3), 180–202. https://doi.org/10.1002/jobm.202000537.

(17) Manfredonia, I.; Incarnato, D. Structure and Regulation of Coronavirus Genomes: State-of-the-Art and Novel Insights from SARS-CoV-2 Studies. *Biochem. Soc. Trans.* **2021**, *49* (1), 341–352. https://doi.org/10.1042/BST20200670.

(18) Brant, A. C.; Tian, W.; Majerciak, V.; Yang, W.; Zheng, Z. M. SARS-CoV-2: From Its Discovery to Genome Structure, Transcription, and Replication. *Cell Biosci.* **2021**, *11* (1). https://doi.org/10.1186/s13578-021-00643-z.

(19) Kung, Y.-A.; Lee, K.-M.; Chiang, H.-J.; Huang, S.-Y.; Wu, C.-J.; Shih, S.-R. Molecular Virology of SARS-CoV-2 and Related Coronaviruses. *Microbiol. Mol. Biol. Rev.* **2022**, *86* (2). https://doi.org/10.1128/mmbr.00026-21.

(20) Holoubek, J.; Bednářová, K.; Haviernik, J.; Huvarová, I.; Dvořáková, Z.; Crossed D Signerný, J.; Outlá, M.; Salát, J.; Konkol'Ová, E.; Boura, E.; Růžek, D.; Vorlíčková, M.; Eyer, L.; Renčiuk, D. Guanine Quadruplexes in the RNA Genome of the Tick-Borne Encephalitis Virus: Their Role as a New Antiviral Target and in Virus Biology. *Nucleic Acids Res.* **2022**, *50* (8), 4574–4600. https://doi.org/10.1093/nar/gkac225.

(21) Fleming, A. M.; Ding, Y.; Alenko, A.; Burrows, C. J. Zika Virus Genomic RNA Possesses Conserved G-Quadruplexes Characteristic of the Flaviviridae Family. *ACS Infect. Dis.* **2016**, *2* (10), 674–681. https://doi.org/10.1021/acsinfecdis.6b00109.

(22) Jamaluddin, N. D.; Mazlan, N. F.; Tan, L. L.; Yusof, N. Y. M.; Khalid, B. G-Quadruplex Microspheres-Based Optical RNA Biosensor for Arthropod-Borne Virus Pathogen Detection: A Proof-of-Concept with Dengue Serotype 2. *Int. J. Biol. Macromol.* **2022**, *199*, 1–9. https://doi.org/10.1016/j.ijbiomac.2021.12.047.

(23) Piekna-Przybylska, D.; Sullivan, M. A.; Sharma, G.; Bambara, R. A. U3 Region in the HIV-1 Genome Adopts a G-Quadruplex Structure in Its RNA and DNA Sequence. *Biochemistry* **2014**, *53* (16), 2581–2593. https://doi.org/10.1021/bi4016692.

(24) Ruggiero, E.; Richter, S. N. Survey and Summary G-Quadruplexes and G-Quadruplex Ligands: Targets and Tools in Antiviral Therapy. *Nucleic Acids Research*. March 15, 2018, pp 3270–3283. https://doi.org/10.1093/nar/gky187.

(25) Metifiot, M.; Amrane, S.; Litvak, S.; Andreola, M. L. Survey and Summary G-Quadruplexes in Viruses: Function and Potential Therapeutic Applications. *Nucleic Acids Res.* **2014**, *42* (20), 12352–12366. https://doi.org/10.1093/nar/gku999.

(26) Tan, J.; Vonrhein, C.; Smart, O. S.; Bricogne, G.; Bollati, M.; Kusov, Y.; Hansen, G.; Mesters, J. R.; Schmidt, C. L.; Hilgenfeld, R. The SARS-Unique Domain (SUD) of SARS Coronavirus Contains Two Macrodomains That Bind G-Quadruplexes. *PLoS Pathog.* **2009**, *5* (5), e1000428. https://doi.org/10.1371/journal.ppat.1000428.

(27) Hognon, C. C.; Miclot, T.; Iriepa, C. G.; Francés-Monerris, A.; Grandemange, S.; Terenzi, A.; Marazzi, M.; Barone, G.; Monari, A.; Garcia-Iriepa, C.; Francés-Monerris, A.; Grandemange, S.; Terenzi, A.; Marazzi, M.; Barone, G.; Monari, A. Role of RNA Guanine Quadruplexes in Favoring the Dimerization of SARS Unique Domain in Coronaviruses. *J. Phys. Chem. Lett.* **2020**, *11* (14), 5661–5667. https://doi.org/10.1021/acs.jpclett.0c01097.

(28) Ruggiero, E.; Zanin, I.; Terreri, M.; Richter, S. N. G-Quadruplex Targeting in the Fight against Viruses: An Update. *Int. J. Mol. Sci.* **2021**, *22* (20), 10984. https://doi.org/10.3390/ijms222010984.

(29) Qin, G.; Zhao, C.; Liu, Y.; Zhang, C.; Yang, G.; Yang, J.; Wang, Z.; Wang, C.; Tu, C.; Guo, Z.; Ren, J.; Qu, X. RNA G-Quadruplex Formed in SARS-CoV-2 Used for COVID-19 Treatment in Animal Models. *Cell Discov.* **2022**, *8* (1). https://doi.org/10.1038/s41421-022-00450-x.

(30) Abiri, A.; Lavigne, M.; Rezaei, M. M.; Nikzad, S. S.; Zare, P.; Mergny, J.-L. L.; Rahimi, H.-R. R.; Peyman, Z.; Mergny, J.-L. L.; Rahimi, H.-R. R. Unlocking G-Quadruplexes as Antiviral Targets. *Pharmacol. Rev.* **2021**, *73* (3), 897–923. https://doi.org/10.1124/pharmrev.120.000230.

(31) Fay, M. M.; Lyons, S. M.; Ivanov, P. RNA G-Quadruplexes in Biology: Principles and Molecular Mechanisms. *J. Mol. Biol.* **2017**, *429* (14), 2127–2147. https://doi.org/10.1016/j.jmb.2017.05.017.

(32) Fonseca Guerra, C.; Bickelhaupt, F. M.; Snijders, J. G.; Baerends, E. J. The Nature of the Hydrogen Bond in DNA Base Pairs: The Role of Charge Transfer and Resonance Assistance. *Chem. - A Eur. J.* **1999**, *5* (12), 3581–3594. https://doi.org/10.1002/(SICI)1521-3765(19991203)5:12<3581::AID-CHEM3581>3.0.CO;2-Y.

(33) Zaccaria, F.; Paragi, G.; Fonseca Guerra, C. The Role of Alkali Metal Cations in the Stabilization of Guanine Quadruplexes: Why K+ Is the Best. *Phys. Chem. Chem. Phys.* **2016**, *18* (31), 20895–20904. https://doi.org/10.1039/c6cp01030j.

(34) Nieuwland, C.; Zaccaria, F.; Fonseca Guerra, C. Understanding Alkali Metal Cation Affinities of Multi-Layer Guanine Quadruplex DNA. *Phys. Chem. Chem. Phys.* **2020**, *22* (37), 21108–21118. https://doi.org/10.1039/d0cp03433a.

(35) Kharel, P.; Becker, G.; Tsvetkov, V.; Ivanov, P. Properties and Biological Impact of RNA G-Quadruplexes: From Order to Turmoil and Back. *Nucleic Acids Res.* **2020**, *48* (22), 12534–12555. https://doi.org/10.1093/nar/gkaa1126.

(36) Karsisiotis, A. I.; Hessari, N. M.; Novellino, E.; Spada, G. P.; Randazzo, A.; da Silva, M. W. Topological Characterization of Nucleic Acid G-Quadruplexes by UV Absorption and Circular Dichroism. *Angew. Chem. - Int. Ed.* **2011**, *123*, 10833–10836.

(37) Vorlíčková, M.; Kejnovská, I.; Bednářová, K.; Renčiuk, D.; Kypr, J. Circular Dichroism Spectroscopy of DNA: From Duplexes to Quadruplexes. *Chirality* **2012**, *24* (9), 691–698. https://doi.org/10.1002/chir.22064.

(38) Kypr, J.; Kejnovská, I.; Renč Iuk, D.; Vorlíč, M. Circular Dichroism and Conformational Polymorphism of DNA. *Nucleic Acids Res.* **2009**, *37* (6), 1713–1725. https://doi.org/10.1093/nar/gkp026.

(39) Gattuso, H.; Spinello, A.; Terenzi, A.; Assfeld, X.; Barone, G.; Monari, A. Circular Dichroism of DNA G-Quadruplexes: Combining Modeling and Spectroscopy to Unravel Complex Structures. *J. Phys. Chem. B* **2016**, *120* (12), 3113–3121. https://doi.org/10.1021/acs.jpcb.6b00634.

(40) Zhao, C.; Qin, G.; Niu, J.; Wang, Z.; Wang, C.; Ren, J.; Qu, X. Targeting RNA G-Quadruplex in SARS-CoV-2: A Promising Therapeutic Target for COVID-19? *Angew. Chemie - Int. Ed.* **2021**, *60* (1), 432–438. https://doi.org/10.1002/anie.202011419.

(41) Liu, G.; Du, W.; Sang, X.; Tong, Q.; Wang, Y.; Chen, G.; Yuan, Y.; Jiang, L.; Cheng, W.; Liu, D.; Tian, Y.; Fu, X. RNA G-Quadruplex in TMPRSS2 Reduces SARS-CoV-2 Infection. *Nat. Commun.* **2022**, *13* (1). https://doi.org/10.1038/s41467-022-29135-5.

(42) Ji, D.; Juhas, M.; Tsang, C. M.; Kwok, C. K.; Li, Y.; Zhang, Y. Discovery of G-Quadruplex-Forming Sequences in SARS-CoV-2. *Brief. Bioinform.* **2021**, *22* (2), 1150–1160. https://doi.org/10.1093/bib/bbaa114.

(43) Miclot, T.; Hognon, C.; Bignon, E.; Terenzi, A.; Marazzi, M.; Barone, G.; Monari, A. Structure and Dynamics of RNA Guanine Quadruplexes in SARS-CoV-2 Genome. Original Strategies against Emerging Viruses. *J. Phys. Chem. Lett.* **2021**, *12* (42), 10277–10283. https://doi.org/10.1021/acs.jpclett.1c03071.

(44) Bouvet, M.; Lugari, A.; Posthuma, C. C.; Zevenhoven, J. C.; Bernard, S.; Betzi, S.; Imbert, I.; Canard, B.; Guillemot, J. C.; Lécine, P.; Pfefferle, S.; Drosten, C.; Snijder, E. J.; Decroly, E.; Morelli, X. Coronavirus Nsp10, a Critical Co-Factor for Activation of Multiple Replicative Enzymes. *J. Biol. Chem.* **2014**, *289* (37), 25783–25796. https://doi.org/10.1074/jbc.M114.577353.

(45) Saramago, M.; Bárria, C.; Costa, V. G.; Souza, C. S.; Viegas, S. C.; Domingues, S.; Lousa, D.; Soares, C. M.; Arraiano, C. M.; Matos, R. G. New Targets for Drug Design: Importance of Nsp14/Nsp10 Complex Formation for the 3'-5' Exoribonucleolytic Activity on SARS-CoV-2. *FEBS J.* **2021**, *288* (17), 5130–5147. https://doi.org/10.1111/febs.15815.

(46) Yan, W.; Zheng, Y.; Zeng, X.; He, B.; Cheng, W. Structural Biology of SARS-CoV-2: Open the Door for Novel Therapies. *Signal Transduct. Target. Ther.* **2022**, *7* (1). https://doi.org/10.1038/s41392-022-00884-5.

(47) Liu, L. Y.; Ma, T. Z.; Zeng, Y. L.; Liu, W.; Mao, Z. W. Structural Basis of Pyridostatin and Its Derivatives Specifically Binding to G-Quadruplexes. *J. Am. Chem. Soc.* **2022**, *144* (26), 11878–11887. https://doi.org/10.1021/jacs.2c04775.

(48) Kim, D. J.; Kim, H. S.; Lee, S. J.; Suh, S. W. Crystal Structure of Thermotoga Maritima SPOUT Superfamily RNA Methyltransferase Tm 1570 in Complex with S-Adenosyl-L-Methionine. *Proteins Struct. Funct. Bioinforma.* **2009**, *74* (1), 245–249. https://doi.org/10.1002/prot.22249.

(49) Phillips, J. C.; Hardy, D. J.; Maia, J. D. C.; Stone, J. E.; Ribeiro, J. V.; Bernardi, R. C.; Buch, R.; Fiorin, G.; Hénin, J.; Jiang, W.; McGreevy, R.; Melo, M. C. R.; Radak, B. K.; Skeel, R. D.; Singharoy, A.; Wang, Y.; Roux, B.; Aksimentiev, A.; Luthey-Schulten, Z.; Kalé, L. V.; Schulten, K.; Chipot, C.; Tajkhorshid, E. Scalable Molecular Dynamics on CPU and GPU Architectures with NAMD. *J. Chem. Phys.* **2020**, *153* (4), 044130. https://doi.org/10.1063/5.0014475.

(50) Phillips, J. C.; Braun, R.; Wang, W.; Gumbart, J.; Tajkhorshid, E.; Villa, E.; Chipot, C.; Skeel, R. D.; Kalé, L.; Schulten, K. Scalable Molecular Dynamics with NAMD. *J. Comput. Chem.* **2005**, *26* (16), 1781–1802. https://doi.org/10.1002/jcc.20289.

(51) Webba da Silva, M.; Trajkovski, M.; Sannohe, Y.; Hessari, N. M. ani; Sugiyama, H.; Plavec, J. Design of a G-Quadruplex Topology through Glycosidic Bond Angles. *Angew. Chemie - Int. Ed.* **2009**, *48* (48), 9167–9170. https://doi.org/10.1002/anie.200902454.

(52) Huang, H.; Suslov, N. B.; Li, N. S.; Shelke, S. A.; Evans, M. E.; Koldobskaya, Y.; Rice, P. A.; Piccirilli, J. A. A G-Quadruplex-Containing RNA Activates Fluorescence in a GFP-like Fluorophore. *Nat. Chem. Biol.* **2014**, *10* (8), 686–691. https://doi.org/10.1038/nchembio.1561.

.
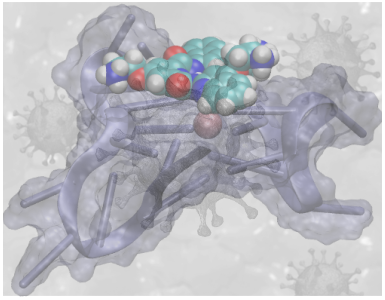
Table of Content